International Journal of Engineering and Geosciences
https://dergipark.org.tr/en/pub/ijeg
e-ISSN 2548-0960

Assessment of Positional Accuracy in Maps Derived Using UAV_PPK, UAV Network RTK, RTK-GNSS, and TUSAGA-Active Techniques

Eren Gürsoy Özdemir [*1], **Emirhan Deniz** [1], **Melisa Hezer** [1]

[1] *Bartın University, Department of Architecture and Urban Planning, Bartın, Türkiye, eozdemir@bartin.edu.tr, emirdnz0761@gmail.com, melisa.hzr@gmail.com*

Cite this study: Özdemir, E.G., Deniz, E., & Hezer, M. (2026). Assessment of Positional Accuracy in Maps Derived Using UAV_PPK, UAV Network RTK, RTK-GNSS, and TUSAGA-Active Techniques. International Journal of Engineering and Geosciences, 11(1), 226-238.

https://doi.org/10.26833/ijeg.1686266

Keywords
Unmanned Aerial Vehicles
PPK-based positioning
Surveying techniques
RTK positioning
Accuracy assessment

Research Article

Received:29.04.2025
1.Revised: 28.06.2025
2.Revised: 16.07.2025
Accepted:25.08.2025
Published:01.02.2026

Abstract

Accurate spatial positioning is essential for many geospatial applications, particularly those requiring high precision. This study evaluates the positional accuracy of maps derived from Unmanned Aerial Vehicle (UAV) data by comparing them with Ground Control Points (GCPs) established using a high-precision electronic total station. Four positioning methods were assessed: Real-Time Kinematic (RTK), TUSAGA-Active (Turkish National Permanent GNSS Network – Active), UAV Post-Processed Kinematic (UAV_PPK), and UAV Network RTK. Accuracy was evaluated regarding horizontal and vertical deviations using standard deviation (SD) and root mean square error (RMSE) metrics. Among the tested methods, RTK demonstrated the highest positional accuracy under the tested conditions, whereas UAV_PPK exhibited the lowest, particularly in vertical positioning. RTK consistently yielded horizontal and vertical RMSE values below 25 mm, while UAV_PPK produced errors exceeding 60 mm in horizontal and reaching up to 115 mm in vertical components. These findings indicate that although UAV-based techniques provide operational efficiency, integrating accurately surveyed GCPs remains critical for achieving reliable spatial accuracy. The study emphasizes the importance of selecting appropriate positioning methods based on project-specific accuracy requirements and supports further research to optimize UAV-based mapping workflows.

1. Introduction

The continuous growth of the global population significantly contributes to the unsustainable consumption of natural resources. This overexploitation and environmental degradation have led to serious global consequences. To address these challenges, researchers employ a range of methods—including Remote Sensing (RS) platforms, terrestrial surveys, and aerial photogrammetry—to collect geospatial data, plan surveys, and monitor environmental conditions in order to better understand and manage natural systems [1,2].

Surveying is vital in generating high-precision topographic data for natural and human-modified environments. Tools such as total stations and Global Navigation Satellite System (GNSS) receivers are commonly used to collect position and elevation data, forming detailed three-dimensional terrain models [3]. These instruments are known for their high accuracy and reliability [4]. However, terrestrial surveying is often labor-intensive, costly, time-consuming, and subject to individual interpretation, as it requires the manual collection of each data point—making the results highly dependent on the surveyor's experience [5,6].

Technological advancements, particularly in satellite systems and GNSS-based techniques, have improved the precision of spatial data acquisition. Absolute and relative positioning are the two principal approaches, with Real-Time Kinematic (RTK) offering high-accuracy results using a single reference station. However, RTK accuracy decreases with distance due to atmospheric interference [7,8]. Network RTK overcomes these limitations by utilizing multiple reference stations, providing consistent positional accuracy across wider areas [9]. In Türkiye, the Turkish National Permanent GNSS Network-Active (TUSAGA-Active) system is a well-established Network RTK infrastructure supporting various geodetic applications [10].

More recently, Unmanned Aerial Vehicles (UAVs) have emerged as practical tools for geospatial data collection, capable of capturing detailed spatial features with speed and efficiency [11–13]. UAVs are aerial platforms without onboard pilots. They can be remotely controlled or operated autonomously using pre-programmed flight paths and automation systems. Their growing use across various disciplines is driven by advantages such as low maintenance and operational costs, flexible hardware configurations, and rapid data acquisition capabilities. The appeal of UAVs is further enhanced by their affordability, adaptability to specific user needs, and the elimination of human risk in hazardous missions [14,15]. Moreover, the automation integrated into image acquisition and processing stages enables efficient and accurate field data collection, offering substantial time and cost savings. This also minimizes the exposure of field personnel to environmental risks and facilitates the rapid generation of topographic products such as Digital Elevation Models (DEMs) and orthophotos [16].

However, the accuracy of UAV-derived data, particularly point cloud products, remains a critical concern in precision-dependent applications such as engineering, infrastructure design, and forestry. As a result, robust ground control and validation processes are essential to ensure the spatial accuracy of photogrammetric outputs [17,18].

Evaluating these datasets through ground-based measurements enhances the reliability and scientific value of UAV applications. Today, UAV technology is widely employed in diverse fields, including urban mapping; modeling of dams, quarries, and disaster sites; cadastral surveying; volume calculations; agricultural and forestry practices; deformation monitoring; documentation and mapping of cultural heritage sites and multi-purpose land classification for engineering applications [19–27].

In aerial photogrammetry, Ground Control Points (GCPs) are fundamental elements that ensure the alignment of map features with their accurate geodetic coordinates. GCPs, determined through geodetic methods, play a critical role in the geometric correction of imagery. The number and spatial distribution of GCPs directly influence the positional accuracy of photogrammetric outputs. In UAV-based photogrammetry, accurately determining the optimal number and placement of GCPs provides significant advantages in terms of time efficiency, cost reduction, and labor requirements [28-30].

Although previous studies have examined the impact of GCP number and distribution on photogrammetric outputs [31,32], limited research has comparatively assessed the accuracy of GCPs established through different measurement techniques under field conditions. This gap highlights the need for a systematic evaluation of GCP quality across terrestrial and aerial methods to ensure optimal integration in geospatial workflows.

This study aims to evaluate the positional accuracy of GCPs established via traditional terrestrial surveying by comparing them with GNSS and UAV photogrammetry coordinates. It is hypothesized that while each method produces georeferenced outputs suitable for diverse applications, integrating UAV and GNSS data—when validated against high-accuracy terrestrial measurements—can improve positional precision in geospatial products.

2. Method

2.1. Study Area

Ulus District is a notable geographical entity within the Western Black Sea subregion of Türkiye's Black Sea Region. Situated in Bartın Province, Ulus is the only inland district of the province, lacking a coastal boundary and positioned further inland. Covering an area of approximately 713 km^2, the district has an average elevation of around 200 meters above sea level, with specific areas reaching elevations of up to 1,200 meters due to the rugged topography of the Küre Mountains. Safranbolu District of Karabük Province borders Ulus to the south, Pınarbaşı and Azdavay districts of Kastamonu Province to the east, Kurucaşile District to the north, and the central district of Bartın to the west [33].

The study area comprises Bartın University's Ulus Vocational School campus, located in the Kaldırım Neighborhood of Ulus District, on parcel 34 of block 232. The study area is positioned within the Universal Transverse Mercator (UTM) coordinate system, Zone 36T, WGS 84 datum, and spans from 469,600 to 469,750 meters easting and 4,605,500 to 4,605,600 meters northing, encompassing a total area of 5,397 m^2. The site is characterized by the mild and humid climatic conditions typical of the Black Sea region, as informed by long-term meteorological data from the Bartın meteorological station, situated approximately 30 meters from the campus. Analysis of 60 years of data (1960–2020) indicates an average annual precipitation of 1,043.8 mm, an average annual temperature of 12.8°C, and an average annual maximum temperature of 19.0°C [34]. The study area is illustrated in Figure 1.

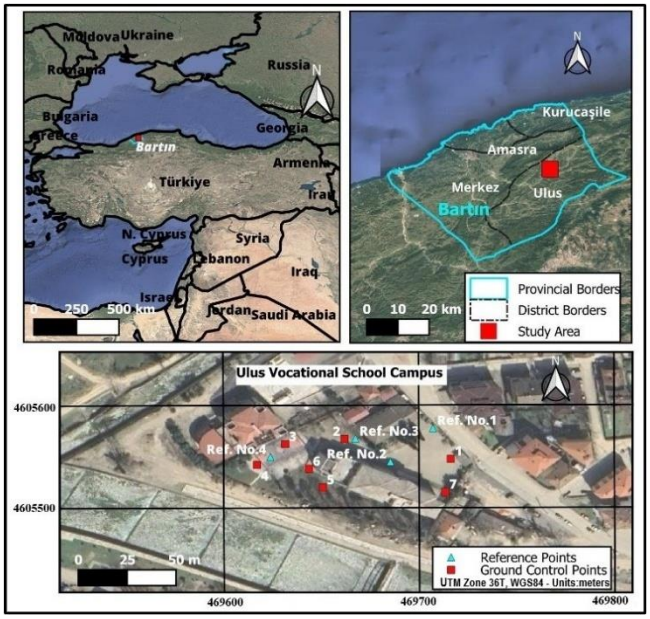

Figure 1. Study Area

2.2. Field Studies

This study employed four reference points (Ref No.) to assess the reliability of measurements for evaluating the positional accuracy obtained from various surveying techniques utilized in precise positioning and spatial data generation. Within this system, the horizontal components are denoted as X (Easting) and Y (Northing), representing the east-west and north-south directions, respectively, while the vertical component, H, represents orthometric height, defined as the height above the geoid, derived using GNSS observations corrected with the Turkey Geoid Model-2020 (TG20).

These reference points are within the campus area and were established before the central survey through static GNSS observations conducted at three different sessions, each lasting three hours. The final coordinates and their corresponding standard deviation (SD) values, derived through post-processing and evaluation, are presented in Table 1.

Table 1. Mean Coordinates and SD Values of GCPs

Point No	X (m)	Y (m)	H (m)	SD. X (mm)	SD. Y (mm)	SD. H (mm)
Ref No. 1	4605586.477	4696 95.105	173.486	3	4	6
Ref No. 2	4605563.596	4696 73.232	172.958	6	9	10
Ref No. 3	4605579.515	4696 55.383	172.849	10	9	12
Ref No. 4	4605567.095	4696 11.802	173.081	7	8	13

Seven GCPs were established within the study area to ensure homogeneous spatial distribution. To achieve high-accuracy measurements, the placement of the GCPs prioritized uninterrupted GNSS signal reception, favoring locations with an unobstructed view of the sky. Furthermore, these points were permanently fixed to maintain stability throughout the study. Each GCP was marked with a target board measuring 50 cm by 70 cm, composed of high-contrast colors to facilitate easy identification during field surveys. A representative image from the field measurements during the establishment of GCPs is presented in Figure 2.

Figure 2. Field Works

The precise coordinates of the GCPs were determined using a total station, a terrestrial surveying instrument. Unlike GNSS systems, which can be adversely affected by atmospheric conditions and signal delays over short baselines—total stations rely on direct line-of-sight measurements, making them less susceptible to environmental obstructions and more suitable for variable field conditions, during the survey process, fixed Ref. No. 1, 2, 3, and 4 were used as benchmarks. The instrument was set up on these reference points, and measurements were taken by sighting the other GCPs to obtain angular, distance, and coordinate data for each location. All measurements were conducted using a Topcon ES 107 model total station to ensure high horizontal and vertical positioning accuracy. The Topcon ES 107 total station, offering 7" angular accuracy and a distance measurement accuracy of ± (2 mm + 2 ppm) using a standard prism, was used for precise GCP collection [35]. The coordinates of each point were calculated based on repeated terrestrial measurements conducted over three independent sessions. The spatial distribution of the points is illustrated in Figure 3.

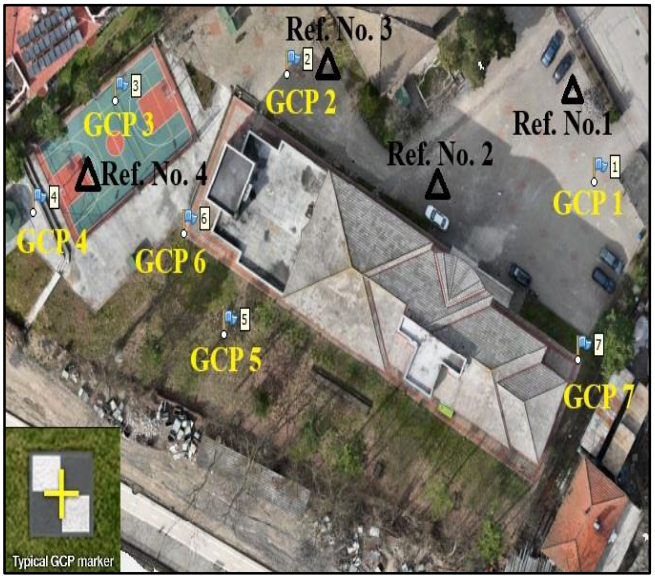

Figure 3. Reference and GCPs Facility in Ulus Vocational School Campus

2.3. GCPs Positioning via Multiple Surveying Techniques

2.3.1. Real-Time Kinematic (RTK) Based Applications

RTK-GNSS enables precise positioning by providing real-time differential corrections. In this methodology, the raw GNSS data from a reference (base) station is transmitted to a mobile (rover) receiver via a communication network, facilitating immediate coordinate adjustments. For this study, two dual-frequency (L1/L2) GNSS receivers, specifically the Sino GNSS N3 models, were employed—comprising one base station and one rover unit. UHF radio frequency was utilized for communication, ensuring the seamless transmission of correction signals from the base station to the rover receiver without any latency. The SinoGNSS N3 receiver supports multi-constellation tracking (GPS, GLONASS, BeiDou, Galileo) and delivers an accuracy of ±8 mm + 1 ppm (horizontal) and ±15 mm + 1 ppm (vertical) in static mode [36].

2.3.2. TUSAGA Active (CORS-TR) Network

As a second approach in this study, the TUSAGA-Active (CORS-TR) network was utilized to perform coordinate measurements for seven GCPs with 30-second epoch sessions. The measurements were repeated in three separate sessions to enhance the accuracy of the measurements and monitor potential changes over time. A Sino GNSS N3 dual-frequency receiver was employed for the GNSS measurements. During the process of converting the measured height values to orthometric heights, the TG20 was used, which was developed under the "Modernization of the Turkey Height System and Improvement of Gravity Infrastructure Project" coordinated by the General Directorate of Mapping (GDM). This enabled converting the obtained height values from the ellipsoidal surface to the geoid surface, ensuring the appropriate correction.

2.3.3. UAV Surveying via PPK and Network RTK

In this study, coordinate computation using UAV imagery followed a multi-stage photogrammetric workflow. First, aerial images were captured using a pre-defined flight plan considering parameters such as altitude, image overlap, ground sampling distance (GSD), and camera orientation. The collected images were processed using Structure-from-Motion techniques to generate dense point clouds, digital surface models (DSMs), and orthophotos. For georeferencing, both indirect and direct methods were employed: indirect georeferencing involved GCPs accurately measured using geodetic GNSS receivers, while direct georeferencing utilized onboard RTK and PPK GNSS systems. The accuracy of the computed coordinates was influenced by UAV sensor configuration, flight geometry, image processing software (Agisoft Metashape), and terrain characteristics. Accuracy assessment was performed by comparing the UAV-derived coordinates against ground survey measurements, and the three-dimensional positional error was evaluated using the spatial vector RMSE to assess overall geolocation accuracy.

In this study, Post-Processed Kinematic (PPK) techniques were employed as a complementary method to improve real-time positioning accuracy and geospatial data acquisition using an UAV. A GNSS receiver was deployed at the Ref. No. 1 location and integrated with a DJI Mavic 3E UAV to enable the collection of high-precision positional data during flight operations. The DJI Mavic 3E features a 20 MP wide-angle camera with a mechanical shutter and supports RTK positioning via an external RTK module. Under optimal conditions, it provides horizontal and vertical positioning accuracies of approximately ±3 cm and ±5 cm, respectively [37].

To ensure sufficient coverage and image redundancy, the data acquisition was conducted at a planned flight altitude of no less than 70 meters, with 70% forward and 80% side overlap. A total of 129 aerial images were captured at a GSD of 1.7 centimeters. Although the total image footprint covered an area of approximately 47,300 m^2, only the central 5,397 m^2 region was designated as the actual study area for analysis. The UAV flight was carried out at a constant speed of approximately 3.5 m/s to maintain image sharpness and alignment consistency, and all images were successfully processed.

The UAV flight was carried out at a constant speed of approximately 3.5 m/s to ensure image sharpness and alignment consistency, and all images were successfully processed.

Concurrently, a static GNSS observation session was conducted using a Sino GNSS N3 dual-frequency receiver throughout the entire flight—from mission planning to landing. This setup enabled precise post-flight trajectory correction via the PPK method. The UAV, equipped with a PPK-capable receiver, received correction data through a Virtual Reference Station (VRS) service provided by the national CORS network, achieving centimeter-level georeferencing accuracy.

The Paksoy PPK v.1.1.1 software, developed based on the RTKLIB open-source GNSS processing engine, was utilized in the PPK processing stage to derive the UAV trajectory. The reference coordinates (X, Y, H) of Base Point No. 1—defined in the ITRF96 and TUREF 33 coordinate system—were entered into the software and subsequently transformed to WGS84 to ensure consistency with the UAV-captured imagery.

During the post-processing, dual-frequency carrier phase observations (L1 and L2) were employed to enhance the robustness of the positioning solution and reduce ionospheric delay effects. Ambiguity resolution was performed automatically using the LAMBDA (Least-squares Ambiguity Decorrelation Adjustment) algorithm, which is integrated within the RTKLIB framework and seeks fixed-integer solutions to improve positional accuracy.

Cycle slips were identified by analyzing carrier-phase continuity. Affected epochs were either excluded from processing or interpolated when feasible, ensuring the integrity and reliability of the final trajectory data.

Aerial images captured during the flight, UAV telemetry data, and static GNSS observations were processed within the PPK software to assign accurate georeferenced coordinates to each image.

The georeferenced images were imported into Agisoft Metashape version 2.1.3 for advanced photogrammetric processing. The standard workflow steps were followed in sequence, beginning with the Align Photos stage, where tie points were automatically detected, and the relative orientations of the camera positions were estimated. This was followed by the Build Dense Cloud step, in which a high-density 3D point cloud was reconstructed using the previously aligned images. A Digital Elevation Model (DEM) and orthophoto were generated from this dense point cloud with high spatial resolution. To enhance the positional accuracy of the final outputs, RTK measurements obtained immediately before and after the UAV flight were averaged to determine the precise coordinates of the GCPs. These refined GCP coordinates were incorporated during the photo-alignment phase, enabling accurate georeferencing and allowing for spatial transformation and residual error analysis between the model and the control points.

In a subsequent UAV flight conducted within the scope of this study, the Network-RTK method was applied. In contrast to the PPK-based workflow, this approach did not require static GNSS observations from a fixed reference station. Instead, real-time corrections were received via the TUSAGA Active Network, enabling precise positioning during flight without needing an on-site base station. The resulting dataset was processed in Agisoft Metashape version 2.1.3 following the same photogrammetric workflow outlined in Figure 4.

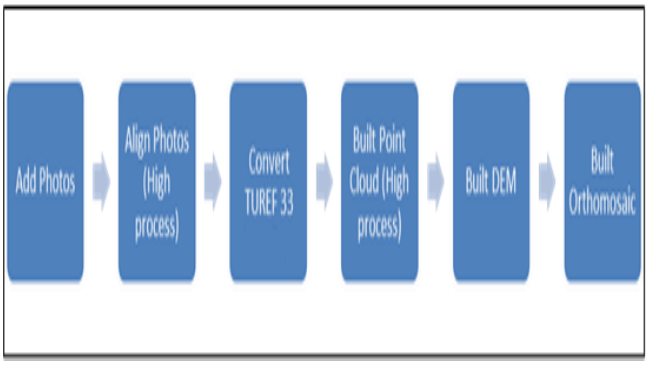

Figure 4. Processing Steps in Agisoft Metashape 2.1.3

The average GCP coordinates were incorporated into the processing workflow following the RTK measurements conducted before and after the UAV flight. After the Align Photos step, GCPs were manually marked and used to perform spatial transformations and error assessments between the images and control points. This georeferencing process transformed the dataset into the ITRF96 coordinate system with Central Meridian Zone 33 (3-degree zone). As a result, high-accuracy outputs—including a dense point cloud, DEM and orthophoto—were successfully generated.

2.4. Accuracy Metrics for GCPs

The positional accuracy of GCPs was rigorously evaluated using two primary statistical metrics: SD, which quantifies measurement precision by analyzing the dispersion of repeated observations, and Root Mean Square Error (RMSE), which provides a comprehensive measure of the discrepancies between measured and reference values. The evaluation framework incorporated multiple measurement repetitions for each GCP, facilitating robust calculations of SD (indicating internal consistency) and RMSE (reflecting overall predictive accuracy). These complementary metrics were systematically analyzed to characterize the spatial error distribution across all surveyed points, with particular attention to elevation (H) uncertainties. These typically exhibit greater variability than topographic surveys' horizontal (X, Y) coordinates. The accuracy metrics are expressed in Equation (1) and Equation (2) below:

$$SD = \sqrt{\frac{1}{N}\sum_{i=1}^{n}(e_i - ME)^2} \quad (1)$$

where

- e_i = Individual measurement
- ME = Mean of measurements
- N = Number of observations

$$RMSE = \sqrt{\frac{1}{N}\sum_{i=1}^{n}(e_i - e_{ref})^2} \quad (2)$$

where

- e_i = Individual measurement
- e_{ref}= Reference(true) measurement
- N = Number of observations

3. Results

3.1. Computation of GCPs using total station measurements

The coordinates of the GCPs were computed based on terrestrial measurements conducted in three independent sessions for each point. The mean coordinate values, SDs, and RMSE values were calculated for every GCP to assess positional accuracy. The measurement sessions and the corresponding statistical analyses are presented in Table 2.

Table 2. Calculation of the coordinates of GCP points using a total station

GCP	Axis	Mean (m)	SD. (mm)	RMSE (mm)
GCP 1	X	4605565.623	1	1
	Y	469704.071	1	1
	H	173.254	2	2
GCP 2	X	4605579.300	2	1
	Y	469649.732	2	2
	H	172.784	2	2
GCP 3	X	4605575.977	2	1

	Y	469619.432	2	1
	H	172.616	3	2
GCP 4	X	4605561.743	1	1
	Y	469604.820	2	1
	H	173.202	2	1
GCP 5	X	4605546.267	2	1
	Y	469638.613	2	1
	H	172.837	3	2
GCP 6	X	4605558.982	2	1
	Y	469631.578	2	1
	H	173.052	3	2
GCP 7	X	4605542.914	2	1
	Y	469701.347	1	1
	H	173.149	3	2

All points' SD and RMSE values are notably low, with none exceeding 3 mm. For points such as GCP 1, GCP 4, and GCP 7, the SD ranges between 1 and 2 mm. In GCP 3, GCP 5, and GCP 6, the SD for the X and Y axes reaches up to 2 mm, while the H coordinate remains within 3 mm. These results indicate a high level of measurement precision and suggest minimal random errors.

3.2. Computation of GCPs using RTK method

For each GCP point, measurements were taken during three separate sessions for the X, Y, and H coordinates, and the mean values were calculated. The SD and RMSE values for the X and Y coordinates range from 3 to 24 mm, while for the H coordinate, they range from 2 to 32 mm. The most significant deviations were observed at GCP 1, with 20 mm in the X and 24 mm in the Y coordinates, and at GCP 5, 32 mm in the H coordinate. The sessions and corresponding calculations are presented in Table 3.

Table 3. Calculation of the coordinates of GCP points using RTK method

GCP	Axis	Mean (m)	SD. (mm)	RMSE (mm)
GCP 1	X	4605565.586	20	16
	Y	469704.076	24	20
	H	173.242	7	5
GCP 2	X	4605579.276	10	9
	Y	469649.750	7	6
	H	172.760	7	5
GCP 3	X	4605575.959	7	6
	Y	469619.416	12	10
	H	172.625	16	13
GCP 4	X	4605561.766	8	6
	Y	469604.867	9	7
	H	173.200	2	2
GCP 5	X	4605546.283	3	3
	Y	469638.573	9	7
	H	172.863	32	26
GCP 6	X	4605558.981	10	8
	Y	469631.521	2	1
	H	173.060	2	2
GCP 7	X	4605542.924	4	3
	Y	469701.302	10	8
	H	173.142	10	8

3.3. Computation of GCPs using TUSAGA Active

GCPs coordination was determined using the TUSAGA-Active method through measurements conducted in three independent sessions. Mean coordinate, SD, and RMSE values were calculated for each point. The conducted sessions and calculations are presented in Table 4.

Table 4. Calculation of the coordinates of GCP points using TUSAGA Active

GCP	Axis	Mean (m)	SD. (mm)	RMSE (mm)
GCP 1	X	4605565.572	44	36
	Y	469704.076	31	25
	H	173.273	67	55
GCP 2	X	4605579.231	50	41
	Y	469649.756	2	1
	H	172.770	66	54
GCP 3	X	4605575.950	7	6
	Y	469619.378	19	16
	H	172.648	23	18
GCP 4	X	4605561.764	15	12
	Y	469604.862	17	14
	H	173.248	33	27
GCP 5	X	4605546.217	40	33
	Y	469638.584	12	10
	H	172.883	79	64
GCP 6	X	4605558.986	29	23
	Y	469631.518	38	31
	H	173.093	2	2
GCP 7	X	4605542.909	16	13
	Y	469701.294	21	17
	H	173.176	33	27

At GCP 5, the SD reaches up to 79 mm for the H (height) axis, while the RMSE values generally remain below 64 mm, with the Y coordinate showing a notably low RMSE of 10 mm. For GCP 3 and 4, the SDs for the X and Y coordinates are consistently below 19 mm and 17 mm, respectively, indicating high accuracy in these coordinates. Remarkably, the RMSE values for the Y coordinates of GCP 2, GCP 5, and GCP 6 are exceptionally low, with GCP 2 achieving an RMSE of 1 mm and GCP 5 and GCP 6 not exceeding 31 mm. The differences in SD and RMSE across the X, Y, and H axes range from 2 to 79 mm, confirming the overall consistency of the measurements. GCP 3 demonstrates the most stable measurements, with RMSE values of 6 mm, 16 mm, and 18 mm for the X, Y, and H axes, respectively, reflecting high precision across all axes.

3.4. Computation of GCPs using UAV's PPK and Network-RTK methods

The PPK solution was completed with a total positional error of approximately 9 cm. As a result of the processing, 60,120.424 points were generated, along with a DEM at a spatial resolution of 3.05 cm/pixel and an orthophoto with a resolution of 1.65 cm/pixel. The GCPs extracted from the orthophoto generated after the

processing steps were compared with the GCP coordinates obtained through ground-based methods.

In the analysis conducted using Network-RTK the process was completed with a total positional error of approximately 7 cm. GCPs extracted from the orthophoto were compared with those obtained through ground-based measurements. As a result of the analysis, a total of 61,768.954 points were generated, along with a DEM at a spatial resolution of 2.09 cm/pixel and an orthophoto at 1.05 cm/pixel resolution. The GCPs derived from the orthophoto generated after the processing steps were compared with those measured in the field. To ensure consistency with flight data in both methods, ellipsoidal heights were used. The orthometric elevations of the obtained GCPs were calculated by subtracting the local geoid undulation value of 33.60 meters from the H-coordinates using the transformation surface model. The coordinates obtained and differences using both methods are presented in Table 5 and shown in Figure 5.

Table 5. The coordinates of GCP's using UAV PPK and UAV Network-RTK methods

Method	GCP	X(m)	Y(m)	H(m)
UAV-PPK	1	4605565.579	469704.041	173.354
	2	4605579.249	469649.789	172.865
	3	4605575.919	469619.474	172.742
	4	4605561.794	469604.899	173.288
	5	4605546.315	469638.708	172.995
	6	4605559.072	469631.511	173.211
	7	4605542.955	469701.391	173.197
UAV-Network RTK	1	4605565.589	469704.075	173.324
	2	4605579.276	469649.785	172.805
	3	4605575.971	469619.465	172.692
	4	4605561.779	469604.895	173.248
	5	4605546.315	469638.648	172.915
	6	4605559.007	469631.561	173.141
	7	4605542.936	469701.321	173.187

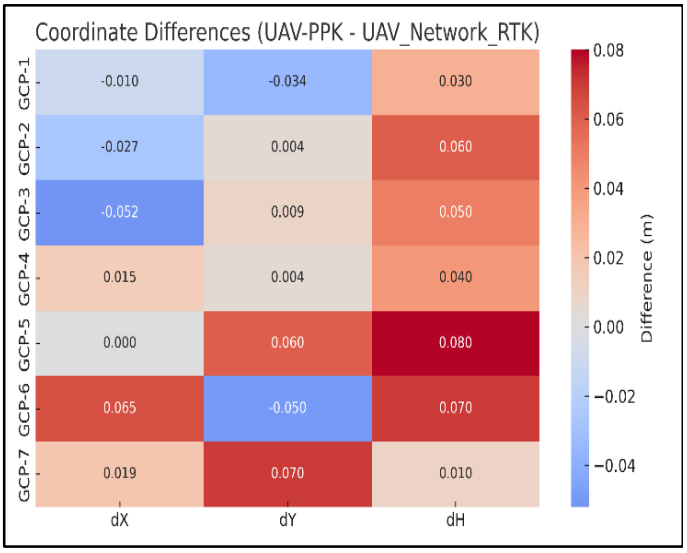

Figure 5. Differences in coordinates of GCP's using UAV PPK and UAV Network-RTK methods

3.5. Assessment of Coordinate Accuracies from Different Methods Against Terrestrial Measurements

In this study, the precise X, Y and H coordinates of seven GNSS control points were determined using terrestrial surveying methods. The positional accuracies obtained from four different GNSS positioning techniques—RTK, TUSAGA-Active, UAV_PPK, and UAV_Network_RTK—were compared against the terrestrial reference data. The discrepancies in the horizontal (X, Y) and vertical (H) components were analyzed in detail (Table 6).

Table 6. Comparison of coordinates obtained from four different methods with reference coordinates

GCP	RTK_dX (mm)	RTK_dY (mm)	RTK_dH(mm)	TUSAGA_dX(mm)	TUSAGA_dY(mm)	TUSAGA_dH(mm)
1	37	-5	12	51	-5	-19
2	24	-18	24	69	-24	14
3	18	16	-9	27	54	-32
4	-23	-47	2	-21	-42	-46
5	-16	40	-26	50	29	-46
6	1	57	-8	-4	60	-41
7	-10	45	7	5	53	-27
GCP	UAV_PPK_dX(mm)	UAV_PPK_dY(mm)	UAV_PPK_dH(mm)	UAV_Network_RTK_dX(mm)	UAV_Network_RTK_dY(mm)	UAV_Network_RTK_dH(mm)
1	44	30	-100	34	-4	-70
2	51	-57	-81	24	-53	-21
3	58	-42	-126	6	-33	-76
4	-51	-79	-86	-36	-75	-46
5	-48	-95	-158	-48	-35	-78
6	-90	67	-159	-25	17	-89
7	-41	-44	-48	-22	26	-38

Additionally, the SD and RMSE values for each method were determined, and accuracy analyses were conducted accordingly (Table 7) and shown in Figure 6.

Table 7. Comparison of metrics obtained from four different methods

Diff.	Method	SD (mm)	RMSE (mm)
dX	RTK	22	21
	TUSAGA	33	40
	UAV_PPK	60	57
	UAV_Network_RTK	31	30
dY	RTK	38	37
	TUSAGA	41	42
	UAV_PPK	59	63
	UAV_Network_RTK	37	41
dH	RTK	16	15
	TUSAGA	21	34
	UAV_PPK	41	115
	UAV_Network_RTK	25	64

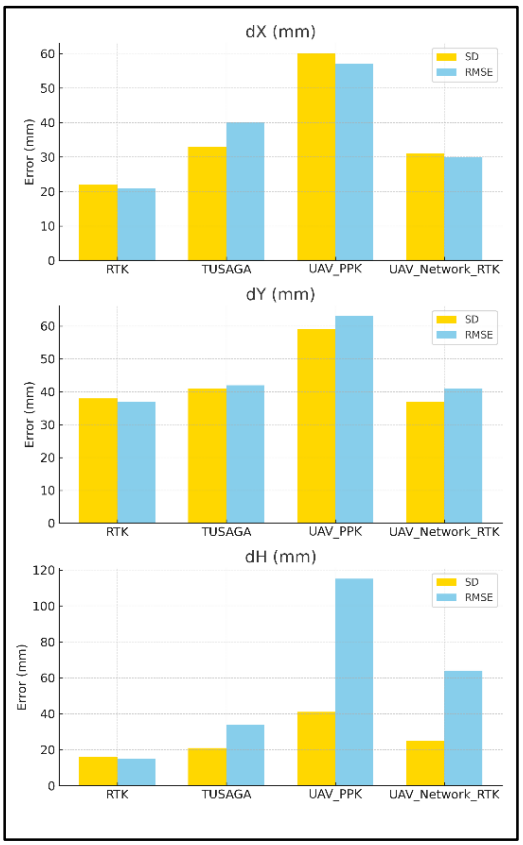

Figure 6. Comparison of SD and RMSE metrics from all methods

In the evaluation based on X-coordinate (horizontal) accuracy, the RTK method demonstrated the lowest error values, emerging as the most reliable positioning technique. The RMSE value for the X-axis using RTK was approximately 21 mm, which is highly suitable for applications requiring precise positioning. The TUSAGA-Active method offered an accuracy level comparable to RTK along the X-axis, with an RMSE value of 40 mm. For the UAV_PPK method, the X-axis RMSE was determined to be 57 mm, indicating one of the highest error deviations among the evaluated methods. This result suggests that UAV_PPK is less reliable for applications demanding high-precision positioning. Meanwhile, the UAV_Network_RTK method exhibited an RMSE value of 30 mm along the X-axis, falling within acceptable error limits and ranking as the second most accurate method after RTK.

In the analysis of Y-coordinate (horizontal) accuracy, the classical RTK method once again demonstrated the highest level of precision, yielding an RMSE of 37 mm. The TUSAGA-Active method showed slightly higher error deviations, with an RMSE of 42 mm and a wider error distribution, particularly at specific locations. The UAV_PPK method recorded a significantly higher RMSE of 63 mm, indicating a relatively poor performance in Y-axis positioning. These results suggest that UAV_PPK may not be suitable for applications requiring high-precision horizontal accuracy and should be cautiously applied in such contexts. The UAV_Network_RTK method yielded an RMSE of 41 mm, achieving accuracy levels similar to TUSAGA-Active but still lower than those of the RTK method.

The most pronounced differences between the tested methods were observed in the analysis of the H coordinate (vertical accuracy). The classical RTK method produced the highest level of accuracy, with an RMSE of 15 mm. Although the TUSAGA-Active method yielded a slightly higher RMSE of 34 mm, it remained within acceptable error thresholds and performed comparably in most cases. The UAV_PPK method exhibited the most considerable vertical deviations, with an RMSE of 115 mm and a notably wide distribution of height errors, indicating a lower level of reliability in vertical positioning. The UAV_Network_RTK method, with an RMSE of 64 mm, performed better than UAV_PPK but demonstrated substantially lower accuracy than the RTK and TUSAGA-Active methods.

To comprehensively assess spatial accuracy, the 3D positional error (R) was calculated for each GCP using the Equation (3). The resulting values for all positioning methods are summarized in Table 8.

$$R = \sqrt{(dX)^2 + (dY)^2 + (dH)^2} \quad (3)$$

Table 8. Comparison of R metric obtained from four different methods

GCP	RTK (mm)	TUSAGA(mm)	UAV_Network_RTK(mm)	UAV_PPK(mm)
GCP 1	39	55	78	113
GCP 2	38	74	62	111
GCP 3	26	68	83	145
GCP 4	52	66	95	127
GCP 5	50	74	98	191
GCP 6	58	73	94	195
GCP 7	47	60	51	77
Mean	44.3	67.1	80.1	137
SD (mm)	10.7	7.4	17.9	43.4
RMSE(mm)	45.4	67.5	81.8	142.8

The comparative analysis of the four positioning methods—RTK, TUSAGA, UAV Network RTK, and UAV PPK—reveals apparent differences in 3D positional accuracy. RTK achieved the lowest mean error (44.3 mm) and RMSE (45.4 mm), indicating the highest overall accuracy among the methods. TUSAGA demonstrated the smallest standard deviation (7.4 mm), suggesting highly consistent results across GCPs, despite a slightly higher mean error (67.1 mm) than RTK. The UAV Network RTK method showed moderate accuracy (mean = 80.1 mm, RMSE = 81.8 mm) but greater variability (SD = 17.9 mm), likely due to in-flight dynamics or GNSS correction delays. UAV PPK exhibited the highest error metrics (mean = 137.0 mm, RMSE = 142.8 mm, SD = 43.4 mm), reflecting lower positional reliability, possibly due to synchronization issues or post-processing limitations. Overall, RTK offered the best accuracy, TUSAGA provided the most consistent performance, and UAV-based methods showed higher variability, particularly in the absence of real-time corrections (Figure 7).

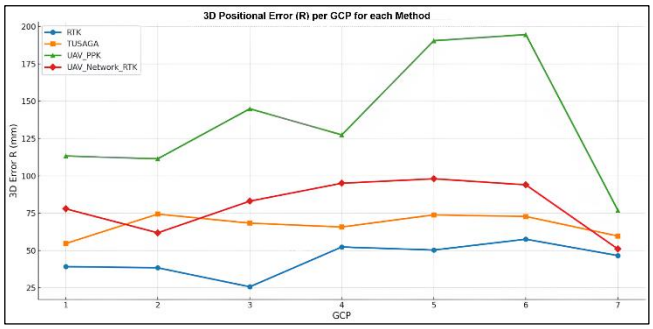

Figure 7. Comparison of 3D positional error from all methods

4. Discussion

The accuracy of UAV-based mapping has been a key focus in recent studies, particularly regarding the performance of various positioning techniques such as RTK, Network RTK, and PPK. Eker et al. (2021) compared UAV-based RTK and PPK techniques over different surface types and reported that Network RTK provided lower positional errors than PPK [38]. Consistent with these findings, our study also demonstrated that RTK produced more accurate results than Network RTK.

Similarly, İnal et al. (2014) examined the performance of classical RTK and Network RTK methods, demonstrating that positional accuracy is directly influenced by the distance to reference stations. Their study reported coordinate discrepancies between the two methods ranging from 0.2 cm to 9.0 cm in the horizontal components (X and Y), with mean errors between ±1.28 cm and ±4.39 cm, and from 0.1 cm to 15.7 cm in the vertical component (H), with corresponding mean errors ranging from ±2.21 cm to ±7.81 cm [39]. These findings are consistent with the results of the present study, confirming that the classical RTK method generally provides superior accuracy compared to Network RTK, particularly in controlling vertical deviations.

Several studies in the literature also indicate that RTK-supported measurements can provide higher accuracy particularly in the vertical (H) component. Padró et al. (2019) reported vertical RMSE values around 15 mm using RTK-based UAV data supported by high-quality GCPs [17]. Similarly, Tomaštík et al. (2017) found that under partially open forest canopy conditions, RTK-enabled UAVs achieved better vertical accuracy (12–18 mm) compared to horizontal accuracy (20–25 mm) [18]. A similar trend was observed in our findings: the RTK method yielded the lowest error values with RMSEs of approximately 21 mm for the X coordinate and 37 mm for the Y coordinate. However, the most notable improvement was observed in the H component. This may be related to the greater effectiveness of RTK systems in correcting vertical measurements and the contribution of nadir-oriented flight geometries to height estimation. In contrast, horizontal accuracy tends to be more affected by factors such as multipath interference, oblique viewing angles, and terrain-related signal distortions. Therefore, the relatively higher vertical accuracy achieved with the RTK method appears to be consistent with previous studies and can be considered technically plausible.

The performance of PPK techniques has also been explored in the literature. Türk et al. (2022) evaluated RTK and PPK performance using the DJI Phantom 4 RTK UAV at a quarry site. Their results indicated positional accuracies of 2.405 cm for RTK and 0.814 cm for PPK, suggesting that PPK may offer advantages in challenging environments such as quarry slopes [40]. However, our findings indicate that, despite using GCP support, the UAV_PPK method resulted in comparatively higher error metric values, particularly in the height component (Figure 8).

This discrepancy can be attributed to multiple factors:

(1) Longer baseline distances between the UAV and the base GNSS station during the flights may have introduced increased positioning error due to decreased satellite geometry strength and potential atmospheric interference;

(2) Signal obstructions from surrounding buildings and vegetation within the urban test area may have caused multipath effects or partial satellite occlusion, particularly affecting height accuracy;

(3) Processing limitations related to post-mission trajectory adjustments and time synchronization between camera exposure and GNSS measurements could also have contributed to vertical deviations.

Thus, the elevated height RMSE observed in the UAV_PPK method is not solely a reflection of the method's limitations but also a consequence of operational and environmental factors, highlighting the sensitivity of this technique to such conditions.

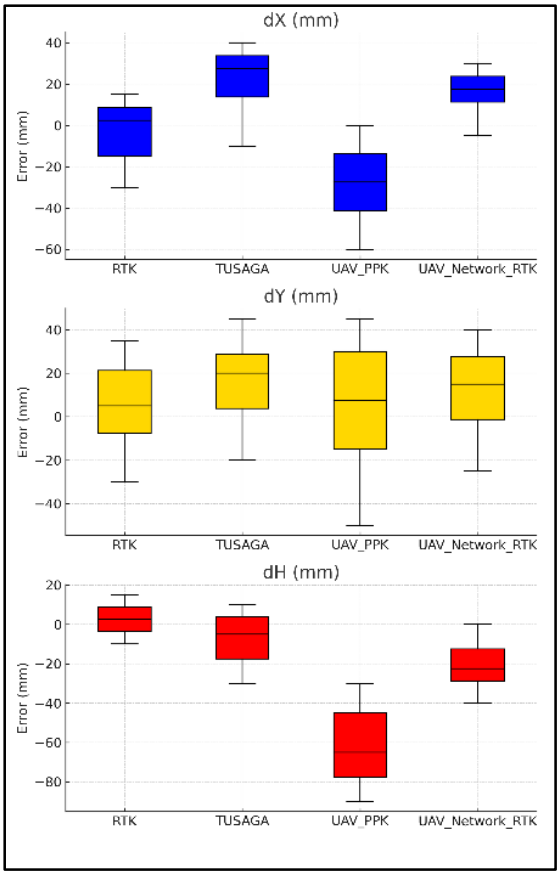

Figure 8. Differences and error metrics of GCP point coordinates across four different methods

Several studies have emphasized the impact of GCP usage on the positional accuracy of orthophotos. Silwal et al. (2022) demonstrated that orthophotos generated with GCP support achieved significantly higher accuracy, reporting an RMSE of 35 mm [41]. Similarly, Güngör et al. (2022) assessed the geometric accuracy of orthophotos produced using CORS-GPS measurements and ten GCPs. They reported RMSE values of ±6.9 cm, ±7.8 cm, and ±10.3 cm in the X, Y, and H coordinate components, respectively [42]. Compared to these studies, the results obtained in the present study exhibit improved spatial accuracy, likely due to the use of precisely measured ground-based reference points, which contributed to minimizing systematic errors.

Flight parameters such as altitude also significantly influence mapping accuracy. Deliry and Avdan (2024) investigated the effects of flight altitude on DSM and orthophoto accuracy, noting an increase in vertical RMSE from 4 cm at 100 m AGL to 6 cm at 170 m AGL, while horizontal RMSE remained stable around 3 cm [6]. In our study, UAV flights were conducted at 70 m AGL, and the resulting accuracy metrics were consistent with the trend observed in the literature, suggesting that lower flight altitudes contribute to enhanced spatial resolution and positional accuracy.

Further comparisons with recent UAV-based mapping studies reveal consistent patterns. Ismael and Henari (2019) [43], reported horizontal and vertical errors of 2.0 cm and 7.5 cm, respectively, using the eBee-SenseFly platform, aligning closely with our study's results achieved through RTK and Network RTK methods. Likewise, Sefercik et al. (2023) reported 3D geolocation accuracies of ±1.1 cm (X), ±2.7 cm (Y), and ±5.7 cm (H) for the DJI Phantom IV Multispectral RTK UAV, while our corresponding RMSE values were slightly higher (3.0 cm, 4.1 cm, and 6.4 cm, respectively) [44]. These minor differences are likely due to variations in GCP distribution, flight parameters, and processing workflows.

Similarly, Pathak et al. (2024) reported RMSE values of 5.37 cm, 4.94 cm, and 6.1 cm in the X, Y, and H coordinate components, respectively, in their UAV-based topographic mapping study supported by GCPs [45]. The results obtained in the present study are closely consistent with these findings, demonstrating a comparable level of positional accuracy and further reinforcing the reliability and robustness of the applied methodology.

Türk and Öcalan (2020) investigated the accuracy of photogrammetric products obtained with UAV-based PPK GNSS systems. Their findings indicated that when GCPs were employed, horizontal and vertical accuracies reached 3.6 cm and 5 cm, respectively. These values deteriorated in the absence of GCPs, especially under longer baseline conditions [46]. Compared to their results, the UAV_PPK method in our study exhibited slightly higher error rates, particularly in vertical accuracy, likely due to differences in baseline lengths and environmental conditions.

In general, among all evaluated methods in our study, the GNSS RTK approach yielded the highest accuracy across the X, Y, and H coordinate components. Although the TUSAGA system achieved comparable performance, it showed slightly greater deviations, particularly in the Y and H directions. Among the UAV-based positioning techniques, UAV_PPK demonstrated the most significant deviations—especially in height (RMSE = 115 mm) —while UAV_Network_RTK offered moderate performance but with notable vertical inaccuracies. These findings collectively confirm that direct RTK correction methods provide the most reliable and precise outcomes for UAV-based high-accuracy mapping.

In addition to the individual X, Y, and H components, the three-dimensional positional accuracy was assessed using the spatial vector R. This analysis revealed that the RTK method not only performed best in individual axes but also yielded the lowest 3D RMSE (45.4 mm), indicating high spatial consistency. Interestingly, while the TUSAGA system showed slightly higher mean errors, it exhibited the lowest standard deviation (7.4 mm) in 3D space, reflecting strong internal consistency. In contrast, UAV_PPK showed the most significant overall 3D error (RMSE = 142.8 mm) and variability (SD = 43.4 mm), whereas UAV_Network RTK demonstrated moderate 3D accuracy with higher fluctuations. These results further validate the advantage of RTK-based positioning methods in ensuring precise and stable spatial geolocation, especially when three-dimensional integrity is critical.

5. Conclusion

This study has highlighted the critical importance of assessing the positional accuracy of maps derived from UAV imagery through a comparative analysis with alternative surveying techniques, including terrestrial measurements and GNSS-based methods. Within this framework, RTK was determined to be the most appropriate method for precision-demanding applications. Although the TUSAGA-Active method delivered acceptable accuracy, UAV-based approaches, especially in height accuracy, demonstrated substantial deviations and should be used cautiously for studies requiring high vertical precision. RTK and TUSAGA methods are recommended. Nonetheless, the UAV_Network_RTK method presents a viable alternative for large-scale surveying projects where extremely high accuracy is not critical due to its time efficiency and advantages in terms of labor savings.

Moreover, this study underscores that although UAV-based methods offer significant operational advantages, they should not be considered a complete substitute for traditional surveying in contexts requiring the highest precision. Instead, a synergistic approach that leverages both UAV and terrestrial/GNSS techniques offers the most robust framework for accurate spatial data generation.

One of the limitations of this study concerns the spatial distribution of ground control points (GCPs) and checkpoints. Due to the compact size of the study area and logistical constraints, the seven control points were concentrated within a relatively limited zone. Although efforts were made to distribute them uniformly to support geometric robustness, this localized clustering

may have introduced a certain degree of spatial bias in the georeferencing accuracy assessment. In future studies, experiments will be conducted over broader and more topographically diverse areas where a more spatially distributed GCP configuration can be considered to improve the reliability of accuracy evaluations and support more generalizable conclusions.

It should also be noted that the present study did not include a no-GCP scenario as a baseline for comparison. While all UAV-based positioning methods assessed here incorporated GCPs to varying extents, future research may benefit from a comparative evaluation of GCP-supported and GCP-free approaches. Such a study is expected to clarify the specific contributions of GCPs to overall positional accuracy and inform decisions regarding ground control requirements under varying mapping conditions.

In addition, future research will explore integrating emerging GNSS technologies—such as PPP-RTK—and advances in onboard UAV positioning systems and machine learning–based error correction techniques. These innovations can potentially enhance the accuracy and reliability of UAV-derived geospatial products. Furthermore, optimizing GCP deployment strategies to reduce field effort without compromising data quality is considered an important direction to improve the operational efficiency and scalability of UAV photogrammetric applications.

Acknowledgement

This research was supported by the TÜBİTAK 2209-A University Students Research Projects Support Program under the project titled “Accuracy Analysis of Maps Generated Using Unmanned Aerial Vehicles (UAVs) and Different Surveying Techniques (1919B012316133).” We express our gratitude to TÜBİTAK BİDEB for their support.

Author contributions

Eren Gürsoy Özdemir: Methodology, Software, Investigation, Validation, Visualization, Writing-Reviewing and Editing. **Emirhan Deniz:** Conceptualization, Investigation, Writing-Original draft preparation, Software, Field study, Investigation. **Melisa Hezer:** Data curation, Writing-Original draft preparation, Software, Field Study, Investigation.

Conflicts of interest

The authors declare no conflicts of interest.

References

1. Clevers, J. G. P. W. (2016). [Review of the book Fundamentals of satellite remote sensing: An environmental approach (2nd ed.), by E. Chuvieco]. International Journal of Applied Earth Observation and Geoinformation, 51, 108–109. https://doi.org/10.1016/j.jag.2016.05.001
2. Serwa, A., & El-Semary, H. H. (2016). Integration of soft computational simulator and strapdown inertial navigation system for aerial surveying project planning. Spatial Information Research, 24(3), 279–290. https://doi.org/10.1007/s41324-016-0027-9
3. Schloderer, G., Bingham, M., Awange, J. L., & Fleming, K. M. (2011). Application of GNSS-RTK derived topographical maps for rapid environmental monitoring: A case study of Jack Finnery Lake (Perth, Australia). Environmental Monitoring and Assessment, 180(1), 147–161. https://doi.org/10.1007/s10661-010-1778-8
4. Manyoky, M., Theiler, P., Steudler, D., & Eisenbeiss, H. (2011, September). Unmanned aerial vehicle in cadastral applications. Paper presented at the International Conference on Unmanned Aerial Vehicle in Geomatics (UAV-g), Zurich, Switzerland. https://doi.org/10.3929/ethz-b-000041977
5. Bangen, S. G., Wheaton, J. M., Bouwes, N., Bouwes, B., & Jordan, C. (2014). A methodological intercomparison of topographic survey techniques for characterizing wadeable streams and rivers. Geomorphology, 206, 343–361. https://doi.org/10.1016/j.geomorph.2013.10.010
6. Deliry, S. I., & Avdan, U. (2024). Accuracy assessment of UAS photogrammetry and structure from motion in surveying and mapping. International Journal of Engineering and Geosciences, 9(2), 165–190. https://doi.org/10.26833/ijeg.1366146
7. Özdemir, E. G. (2022). Bağıl ve mutlak (PPP) konum çözüm yaklaşımı sunan Web-Tabanlı çevrimiçi veri değerlendirme servislerinin farklı gözlem periyotlarındaki performanslarının araştırılması. Geomatik, 7(1), 41–51. https://doi.org/10.29128/geomatik.809826
8. Wanninger, L. (1998). Real-time differential GPS error modelling in regional reference station networks. In F. K. Brunner (Ed.), Advances in positioning and reference frames (pp. 86–92). Springer.
9. Rizos, C., & Han, S. (2003). Reference station network based RTK systems-concepts and progress. Wuhan University Journal of Natural Sciences, 8(2), 566–574. https://doi.org/10.1007/BF02899820
10. Akpınar, B., Aykut, N. O., Dindar, A. A., Gürkan, K., & Gülal, E. (2017). Ağ RTK GNSS Yönteminin Yapı Sağlığı İzleme Çalışmalarında Kullanımı. Afyon Kocatepe Üniversitesi Fen ve Mühendislik Bilimleri Dergisi, 17(3),1030–1040. https://doi.org/10.5578/fmbd.66278
11. Erdoğan, A., & Mutluoglu, Ö. (2020). İnsansız Hava Aracı (İHA) ile Üretilen Şeritvari Haritalardan Kübaj Hesabı. Türkiye İnsansız Hava Araçları Dergisi, 2(2), 61–66.
12. Unger, J., Reich, M., & Heipke, C. (2014). UAV-based photogrammetry: Monitoring of a building zone. The International Archives of the Photogrammetry, Remote Sensing and Spatial

Information Sciences, XL–5, 601–606. https://doi.org/10.5194/isprsarchives-XL-5-601-2014
13. Yakar, M. (2011). Using close range photogrammetry to measure the position of inaccessible geological features. Experimental Techniques, 35(1), 54-59.
14. Azmi, S. M., Ahmad, B., & Ahmad, A. (2014). Accuracy assessment of topographic mapping using UAV image integrated with satellite images. IOP Conference Series: Earth and Environmental Science, 18(1), 012015. https://doi.org/10.1088/1755-1315/18/1/012015
15. Villi, O., & Yakar, M. (2022). İnsansız Hava Araçlarının Kullanım Alanları ve Sensör Tipleri. Türkiye İnsansız Hava Araçları Dergisi, 4(2), 73-100. https://doi.org/10.15317/Scitech.2017.109
16. Nwilag, B. D., Eyoh, A. E., & Ndehedehe, C. E. (2023). Digital topographic mapping and modelling using low altitude unmanned aerial vehicle. Modeling Earth Systems and Environment, 9(2), 1463–1476. https://doi.org/10.1007/s40808-022-01677-z
17. Padró, J.-C., Muñoz, F.-J., Planas, J., & Pons, X. (2019). Comparison of four UAV georeferencing methods for environmental monitoring purposes focusing on the combined use with airborne and satellite remote sensing platforms. International Journal of Applied Earth Observation and Geoinformation, 75, 130–140. https://doi.org/10.1016/j.jag.2018.10.018
18. Tomaštík, J., Mokroš, M., Surový, P., Grznárová, A., & Merganič, J. (2019). UAV RTK/PPK Method—An Optimal Solution for Mapping Inaccessible Forested Areas? Remote Sensing, 11(6). https://doi.org/10.3390/rs11060721
19. Kökhan, S., & Engin, M. A. (2024). İnsansız Hava Araçları ile Orman Yangınlarının Tespitinde Görüntü İşleme ve Yapay Zekâ Tabanlı Otomatik Bir Model. Duzce University Journal of Science and Technology, 12(2), 762–775. https://doi.org/10.29130/dubited.1103375
20. Kun, M., & Özcan, B. (2019). Maden ocaklarında insansız hava aracı kullanımı: Örnek bir saha çalışması. Balıkesir Üniversitesi Fen Bilimleri Enstitüsü Dergisi, 21(2), 554–564. https://doi.org/10.25092/baunfbed.624484
21. Mırdan, O., & Yakar, M. (2017). Tarihi Eserlerin İnsansız Hava Aracı ile Modellenmesinde Karşılaşılan Sorunlar. Geomatik, 2(3), 118-125. https://doi.org/10.29128/geomatik.306914
22. Yakar, M., Yıldız, F., Uray, F., & Metin, A. (2010, June). Photogrammetric Measurement of The Meke Lake and Its Environment with Kite Photographs to Monitoring of Water Level to Climate Change. In ISPRS Commission V Mid-Term Symposium (pp. 613-616).
23. Ünel, F. B., Kuşak, L., Yakar, M., & Doğan, H. (2023). Coğrafi bilgi sistemleri ve analitik hiyerarşi prosesi kullanarak Mersin ilinde otomatik meteoroloji gözlem istasyonu yer seçimi. Geomatik, 8(2), 107-123.
24. Yilmaz, H. M., Yakar, M., Mutluoglu, O., Kavurmaci, M. M., & Yurt, K. (2012). Monitoring of soil erosion in Cappadocia region (Selime-Aksaray-Turkey). Environmental Earth Sciences, 66(1), 75-81.
25. Alyilmaz, C., Alyilmaz, S. & Yakar, M. (2010). Measurement of petroglyhps (rock of arts) of Qobustan with close range photogrammetry. International Archives of Photogrammetry, Remote Sensing and Spatial Information Sciences, 38 (Part 5), 29-32.
26. Erdal, K., & Makineci, H. B. (2023). Adaptation analysis of produced 3D models from UAV-SLAM and UAV-TLS data combinations. Mersin Photogrammetry Journal, 5(1), 18-23. https://doi.org/10.53093/mephoj.1269630
27. Varol, F. (2025). Creation of surface model using unmanned aerial vehicle (UAV) photogrammetry in cultural heritage areas: The example of Kilistra Ancient City. International Journal of Engineering and Geosciences, 10(2), 137-150. https://doi.org/10.26833/ijeg.1487818
28. Forlani, G., Dall'Asta, E., Diotri, F., Cella, U. M. di, Roncella, R., & Santise, M. (2018). Quality Assessment of DSMs Produced from UAV Flights Georeferenced with On-Board RTK Positioning. Remote Sensing, 10(2). https://doi.org/10.3390/rs10020311
29. Hastaoğlu, K. Ö., Gül, Y., Poyraz, F., & Kara, B. C. (2019). Monitoring 3D areal displacements by a new methodology and software using UAV photogrammetry. International Journal of Applied Earth Observation and Geoinformation, 83, 101916. https://doi.org/10.1016/j.jag.2019.101916
30. Altuntabak, H., & Ata, E. (2022). Investigation of accuracy of detailed verified by unmanned aerial vehicles with RTK system; The example of Ortakent-Bodrum Area. Advanced UAV, 2(1), 1–10. https://publish.mersin.edu.tr/index.php/uav/article/view/244
31. Shah, M. S. M. Z., Ariff, M. F. M., & Razali, A. F. (2022). Accuracy assessment of airborne mapping based on variation of number and distribution of ground control points. In 2022 IEEE 10th Conference on Systems, Process & Control (ICSPC) (pp. 88–93). IEEE. https://doi.org/10.1109/ICSPC55597.2022.10001799
32. Polat, H., & Ataş, İ. (2024). Accuracy Analysis of Photogrammetric Digital Topographic Map Production: The Case Study of Kuruca Village in Bingöl Center. International Journal of Nature and Life Sciences, 8(2), 241-251. https://doi.org/10.47947/ijnls.1608608
33. Bartın Governorship. (2025). Ulus. http://www.bartin.gov.tr/ulus

34. Turkish State Meteorological Service. (2023). Meteorological data. http://www.mgm.gov.tr
35. Topcon. (2021). Topcon ES Series Total Stations – Product Overview. Topcon Positioning Systems. Retrieved from: http://topconsokkia.ind.in/www/uploads/product_brochur/es-series.pdf
36. SinoGNSS. (2022). N3 GNSS Receiver Datasheet. CHC Navigation. Retrieved from: https://www.comnavtech.com/sp/uploads/soft/20240530/de84c56eec4fd67bcc89d25c7b71d8f5.pdf.
37. DJI. (2022). Mavic 3 Enterprise Series Specifications. DJI Official Website. Retrieved from: https://enterprise.dji.com/mavic-3-enterprise/specs
38. Eker, R., Alkan, E., & Aydın, A. (2021). A Comparative Analysis of UAV-RTK and UAV-PPK Methods in Mapping Different Surface Types. European Journal of Forest Engineering, 7(1), 12–25. https://doi.org/10.33904/ejfe.938067
39. İnal, C., Gündüz, A. M., & Bülbül, S. (2014). Klasik RTK ve Ağ-RTK Yöntemlerinin Karşılaştırılması. Selçuk Üniversitesi Mühendislik, Bilim ve Teknoloji Dergisi, 2(2), 21-30.
40. Türk, Y., Balaban, B., Alkan, E., Çınar, T., & Aydın, A. (2022). Açık maden sahalarında kazı sonrası zemin değişiminin izlenmesinde İHA-tabanlı RTK/PPK yönteminin kullanımı: Düzce-Tatlıdere taş ocağı örneği. Ormancılık Araştırma Dergisi, 9(Özel Sayı), 76–85. https://doi.org/10.17568/ogmoad.1093694
41. Silwal, A., Tamang, S., & Adhikari, R. (2022). Use of unmanned aerial vehicle (UAV) for mapping, and accuracy assessment of the orthophoto with and without using GCPs: A case study in Nepal. Mersin Photogrammetry Journal, 4(2), 45–52. https://doi.org/10.53093/mephoj.1176847
42. Güngör, R., Uzar, M., Atak, B., Yılmaz, O. S., et al. (2022). Orthophoto production and accuracy analysis with UAV photogrammetry. Mersin Photogrammetry Journal, 4(1), 1-6. https://doi.org/10.53093/mephoj.1122615
43. Ismael, R. Q., & Henari, Q. Z. (2019). Accuracy assessment of UAV photogrammetry for large scale topographic mapping. In 2019 International Engineering Conference (IEC) (pp. 1–5). https://doi.org/10.1109/IEC47844.2019.8950607
44. Sefercik, U. G., Kavzoğlu, T., Çölkesen, İ., Nazar, M., et al. (2023). 3D positioning accuracy and land cover classification performance of multispectral RTK UAVs. International Journal of Engineering and Geosciences, 8(2), 119-128. https://doi.org/10.26833/ijeg.1074791
45. Pathak, S., Acharya, S., Bk, S., Karn, G., et al. (2024). UAV-based topographical mapping and accuracy assessment of orthophoto using GCP. Mersin Photogrammetry Journal, 6(1), 1-8. https://doi.org/10.53093/mephoj.1350426
46. Türk, T., & Öcalan, T. (2020). PPK GNSS Sistemine Sahip İnsansız Hava Araçları ile Elde Edilen Fotogrametrik Ürünlerin Doğruluğunun Farklı Yaklaşımlarla İrdelenmesi. Türkiye Fotogrametri Dergisi, 2(1), 22–28.